Supporting Information

Charge Density of Intercalants inside Layered Birnessite Manganese Oxide Nanosheets Determining Zn-ion Storage Capability towards Rechargeable Zn-ion Batteries

*Praeploy Chomkhuntod, Kanit Hantanasirisakul, Salatan Duangdangchote, Nutthaphon Phattharasupakun, and Montree Sawangphruk**

Centre of Excellence for Energy Storage Technology (CEST), Department of Chemical and Biomolecular Engineering, School of Energy Science and Engineering, Vidyasirimedhi Institute of Science and Technology, Rayong 21210, Thailand

*Corresponding author. Tel: +66(0)33-01-4251 Fax: + 66(0)33-01-4445.

E-mail address: montree.s@vistec.ac.th (M. Sawangphruk).

ORCID ID: https://orcid.org/0000-0003-2769-4172

Computational Methods

All calculations reported in this work were performed by Vienna *ab initio* simulation package (VASP) based on the periodic plane-wave density functional theory (DFT).[1-3] The interaction between ion cores and valence electrons was accounted by the projector-augmented wave (PAW) pseudopotentials.[4] The exchange and correlation interactions between electrons were treated within the generalized gradient approximation (GGA) with the Perdev-Burke-Ernzerhof (PBE) parameterization.[5, 6] The additional van der Waals (vdW) contributions were obtained from the semiempirical D2 method of Grimme (DFT-D2).[7] The effect of 3d electron correlation can be improved by considering on-site Coulomb (U) and exchange (J) interactions. On-site Hubbard term U−J values of 3.9 eV were applied for Mn atom.[8, 9] The cut-off energy for the expanded plane-wave basis set was set to 450 eV. The convergence thresholds for full geometry optimizations were set to 10^{-5} eV and 0.02 eV/Å for each electronic and ionic step. The Brillouin zone integration was sampled *via* the Monkhorst–Pack (MP) with the 2×3×4 *k*-points mesh for supercell and 2×3×4 *k*-points mesh for bulk.[10] The calculated relative binding (E_b) energy was obtained from the equation as follows:

$$E_b = E_{Zn/MnO_2} - E_{Zn} - E_{MnO_2}$$

where $E_{Zn/MnO2}$, E_{Zn}, and E_{MnO2} are the total energies of the adsorbed Zn in the MnO_2 structure, the pristine $MMnO_2$ structure, and the bulk Zn, respectively.

Table S1 Elemental analysis, where X=Li, Ca, and Al.

Sample	**X/Mn Ratio**	
	ICP	XRF
Li-MnO_2	0.33	N/A*
Ca-MnO_2	0.15	0.14
Al-MnO_2	0.07	0.07

* Li detection is not applicable with XRF technique.

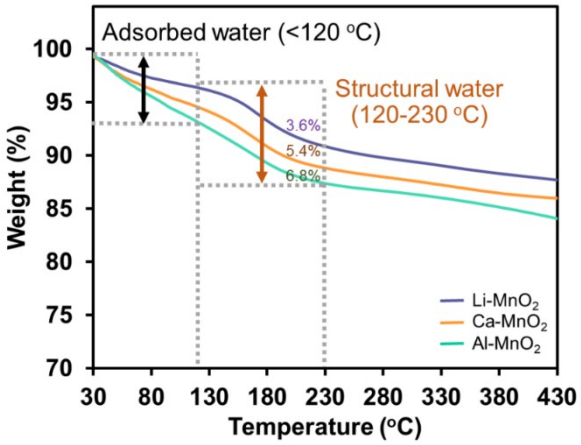

Fig. S1 The TGA curves of the as-prepared MnO_2 at a heating rate of 10 °C min^{-1} under air atmosphere.

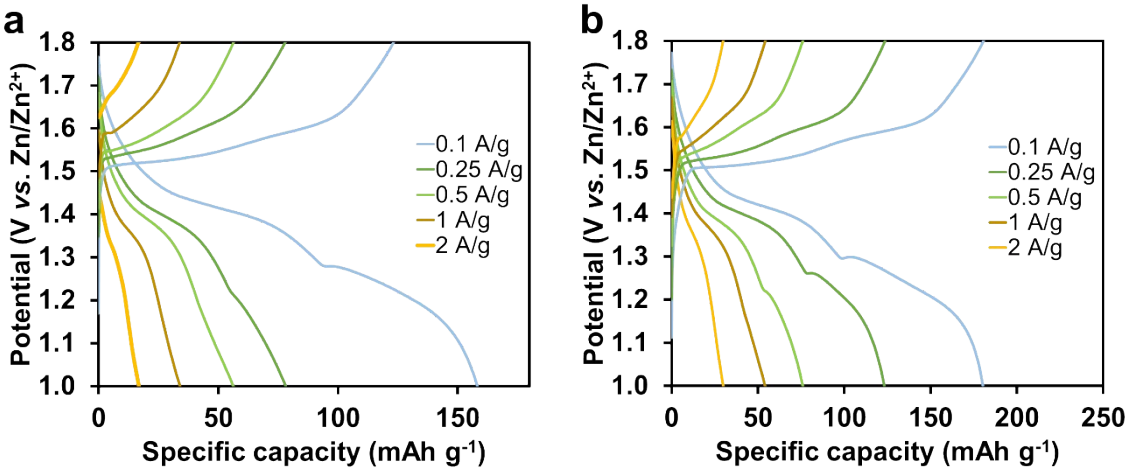

Fig. S2 Galvanostatic charge-discharge profiles at different current densities of (a) Li-MnO_2 and (b) Ca-MnO_2.

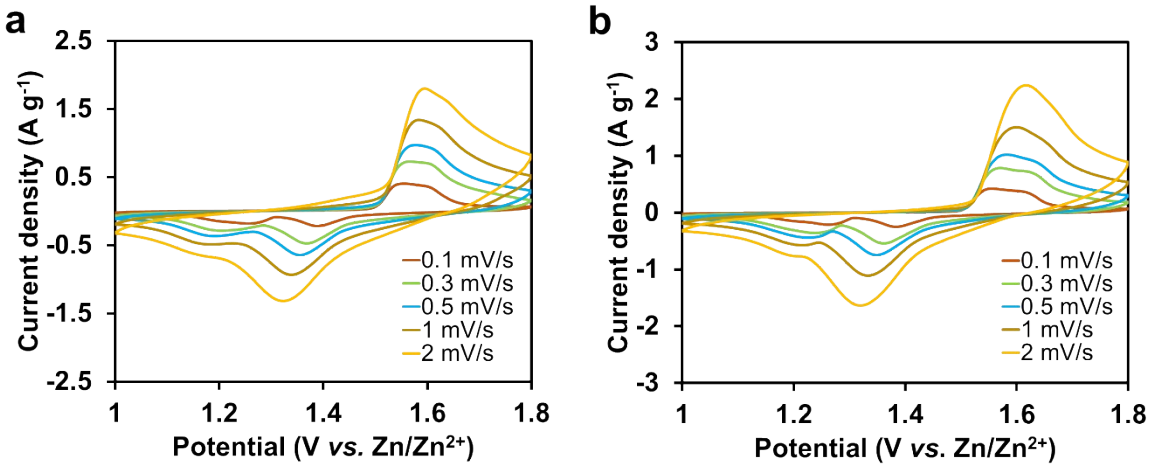

Fig. S3 CV profiles as a function of scan rate of (a) Li-MnO_2 and (b) Ca-MnO_2.

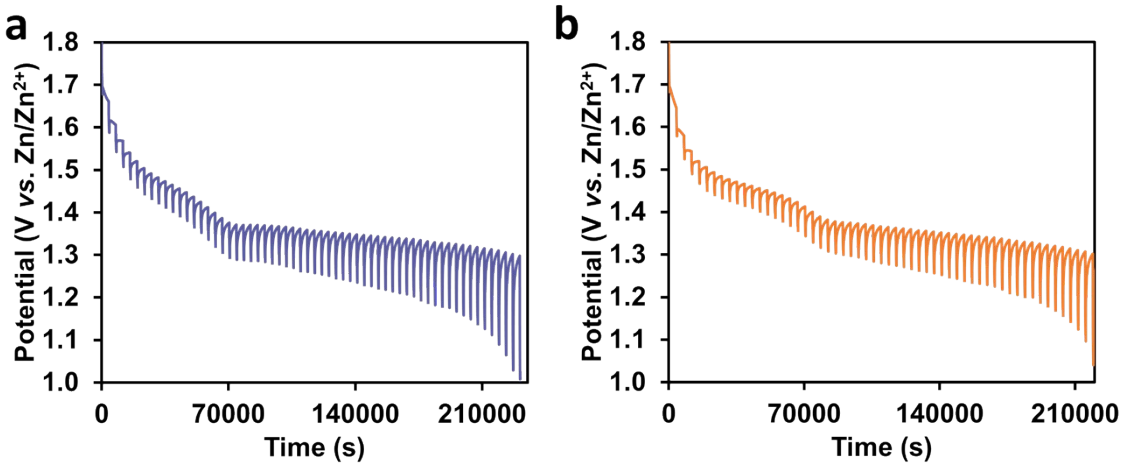

Fig. S4 GITT profiles during discharging process of (a) Li-MnO_2 and (b) Ca-MnO_2.

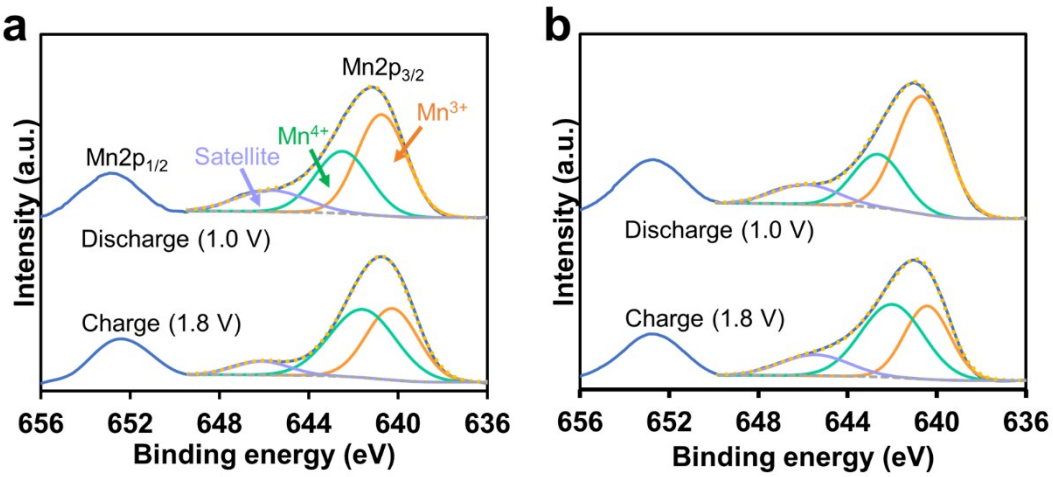

Fig. S5 XPS profiles after charging/discharging process of (a) Li-MnO_2 and (b) Ca-MnO_2.

Table S2 The benchmarking table of capacity and cycling performance for manganese oxide-based cathodes in aqueous Zn-ion batteries.

Sample	Morphology	Electrolyte	Window potential	Capacity	Stability	Ref
α-MnO_2	nanorod	1 M $ZnSO_4$	0.7-2.0 V *vs*. Zn/Zn^{2+}	167 mAh g^{-1} at 42 mA g^{-1}	70% after 30 cycles at 42 mA g^{-1}	[11]
Bi-α-MnO_2	nanowire	2 M $ZnSO_4$ + 0.1 M $MnSO_4$	0.8-1.9 V *vs*. Zn/Zn^{2+}	325 mAh g^{-1} at 0.3 A g^{-1}	90.9% after 2000 cycles at 1 A g^{-1}	[12]
ε-MnO_2	nanosheet	2 M $ZnSO_4$ + 0.5 M $MnSO_4$	1.0-1.8 V *vs*. Zn/Zn^{2+}	183.4 mAh g^{-1} at 0.5 A g^{-1}	83% after 1000 cycles at 5 A g^{-1}	[13]
β-MnO_2	nanofiber	3 M $ZnSO_4$ + 0.2 M $MnSO_4$	1.0-1.8 V *vs*. Zn/Zn^{2+}	288 mAh g^{-1} at 0.05 C	84.3% after 1000 cycles at 2 C	[14]
γ-MnO_2	nanowire /fiber	1 M $ZnSO_4$	1.0-1.8 V *vs*. Zn/Zn^{2+}	219 mAh g^{-1} at 0.5 mA cm^{-2}	37% after 40 cycles at 0.5 mA cm^{-2}	[15]
δ-MnO_2	nanowire	2 M $ZnSO_4$ + 0.1 M $MnSO_4$	1.0-1.8 V *vs*. Zn/Zn^{2+}	<200 mAh g^{-1} at 0.2 A g^{-1}	40% after 700 cycles at 200 mA g^{-1}	[16]
δ-MnO_2/C	nanoflower	2.0 M $ZnSO_4$+ 0.5 M $MnSO_4$	1.0-1.9 V *vs*. Zn/Zn^{2+}	203 mA h g^{-1} at 3 A g^{-1}	61.85% after 1500 cycles at 2 A g^{-1}	[17]
δ-MnO_2	flake	1 M $ZnSO_4$	1.0-1.8 V *vs*. Zn/Zn^{2+}	233 mAh g^{-1} at 100 mA g^{-1}	~ 45% after 50 cycles at 100 mA g^{-1}	[18]
PANI-intercalated δ-MnO_2	grainy	2 M ZnSO4 + 0.1 M MnSO4	1.0-1.8 V *vs*. Zn/Zn^{2+}	110 mA h g^{-1} at 3 A g^{-1}	~83% after 5000 cycles at 2 A g^{-1}	[19]
δ-MnO_2	flake	1 M $ZnSO_4$	1.0-1.8 V *vs*. Zn/Zn^{2+}	252 mAh g^{-1} at 83 mA g^{-1}	~ 44.4 % after 100 cycles at 83 mA g^{-1}	[20]
δ-MnO_2/ graphite	nanoflower	1 M $ZnSO_4$	1.0-1.8 V *vs*. Zn/Zn^{2+}	181 mAh g^{-1} at 200 mA g^{-1}	~ 90% after 100 cycles at 400 mA g^{-1}	[21]
Al-intercalated δ-MnO_2	sheet	2 M $ZnSO_4$	1.0-1.8 V *vs*. Zn/Zn^{2+}	210 mAh g^{-1} at 100 mA g^{-1}	84% after 2000 cycles at 2 A g^{-1}	This work

References

1. Kresse, G.; Hafner, J., Ab initio molecular dynamics for liquid metals. *Phys. Rev. B* **1993,** *47* (1), 558-561.
2. Kresse, G.; Furthmüller, J., Efficiency of ab-initio total energy calculations for metals and semiconductors using a plane-wave basis set. *Comput. Mater. Sci.* **1996,** *6* (1), 15-50.
3. Kresse, G.; Furthmüller, J., Efficient iterative schemes for ab initio total-energy calculations using a plane-wave basis set. *Phys. Rev. B* **1996,** *54* (16), 11169-11186.
4. Kresse, G.; Joubert, D., From ultrasoft pseudopotentials to the projector augmented-wave method. *Phys. Rev. B* **1999,** *59* (3), 1758-1775.
5. Perdew, J. P.; Burke, K.; Ernzerhof, M., Generalized Gradient Approximation Made Simple. *Phys. Rev. Lett.* **1996,** *77* (18), 3865-3868.
6. Perdew, J. P.; Ernzerhof, M.; Burke, K., Rationale for mixing exact exchange with density functional approximations. *J. Chem. Phys.* **1996,** *105* (22), 9982-9985.
7. Stefan, G., Semiempirical GGA-type density functional constructed with a long-range dispersion correction. *J. Comput. Chem.* **2006,** *27* (15), 1787-1799.
8. Anisimov, V. I.; Zaanen, J.; Andersen, O. K., Band theory and Mott insulators: Hubbard U instead of Stoner I. *Phys. Rev. B* **1991,** *44* (3), 943-954.
9. Mueller, T.; Hautier, G.; Jain, A.; Ceder, G., Evaluation of Tavorite-Structured Cathode Materials for Lithium-Ion Batteries Using High-Throughput Computing. *Chem. Mater.* **2011,** *23* (17), 3854-3862.
10. Monkhorst, H. J.; Pack, J. D., Special points for Brillouin-zone integrations. *Phys. Rev. B* **1976,** *13* (12), 5188-5192.

11. Lee, B.; Lee, H. R.; Kim, H.; Chung, K. Y.; Cho, B. W.; Oh, S. H., Elucidating the intercalation mechanism of zinc ions into α-MnO2 for rechargeable zinc batteries. *Chem. Commun.* **2015,** *51* (45), 9265-9268.
12. Ma, K.; Li, Q.; Hong, C.; Yang, G.; Wang, C., Bi Doping-Enhanced Reversible-Phase Transition of α-MnO2 Raising the Cycle Capability of Aqueous Zn–Mn Batteries. *ACS Appl. Mater. Interfaces* **2021,** *13* (46), 55208-55217.
13. Zhang, Y.; Liu, Y.; Liu, Z.; Wu, X.; Wen, Y.; Chen, H.; Ni, X.; Liu, G.; Huang, J.; Peng, S., MnO2 cathode materials with the improved stability via nitrogen doping for aqueous zinc-ion batteries. *J. Energy Chem.* **2022,** *64*, 23-32.
14. Liu, M.; Zhao, Q.; Liu, H.; Yang, J.; Chen, X.; Yang, L.; Cui, Y.; Huang, W.; Zhao, W.; Song, A.; Wang, Y.; Ding, S.; Song, Y.; Qian, G.; Chen, H.; Pan, F., Tuning phase evolution of β-MnO2 during microwave hydrothermal synthesis for high-performance aqueous Zn ion battery. *Nano Energy* **2019,** *64*, 103942.
15. Alfaruqi, M. H.; Mathew, V.; Gim, J.; Kim, S.; Song, J.; Baboo, J. P.; Choi, S. H.; Kim, J., Electrochemically Induced Structural Transformation in a γ-MnO2 Cathode of a High Capacity Zinc-Ion Battery System. *Chem. Mater.* **2015,** *27* (10), 3609-3620.
16. Chen, X.; Li, W.; Zeng, Z.; Reed, D.; Li, X.; Liu, X., Engineering stable Zn-MnO2 batteries by synergistic stabilization between the carbon nanofiber core and birnessite-MnO2 nanosheets shell. *Chem. Eng. J.* **2021,** *405*, 126969.
17. Li, G.; Huang, Z.; Chen, J.; Yao, F.; Liu, J.; Li, O. L.; Sun, S.; Shi, Z., Rechargeable Zn-ion batteries with high power and energy densities: a two-electron reaction pathway in birnessite MnO2 cathode materials. *J. Mater. Chem. A* **2020,** *8* (4), 1975-1985.
18. Alfaruqi, M. H.; Islam, S.; Putro, D. Y.; Mathew, V.; Kim, S.; Jo, J.; Kim, S.; Sun, Y.-K.; Kim, K.; Kim, J., Structural transformation and electrochemical study of layered MnO2 in rechargeable aqueous zinc-ion battery. *Electrochim. Acta* **2018,** *276*, 1-11.
19. Huang, J.; Wang, Z.; Hou, M.; Dong, X.; Liu, Y.; Wang, Y.; Xia, Y., Polyaniline-intercalated manganese dioxide nanolayers as a high-performance cathode material for an aqueous zinc-ion battery. *Nat. Comm.* **2018,** *9* (1), 2906.
20. Alfaruqi, M. H.; Gim, J.; Kim, S.; Song, J.; Pham, D. T.; Jo, J.; Xiu, Z.; Mathew, V.; Kim, J., A layered δ-MnO2 nanoflake cathode with high zinc-storage capacities for eco-friendly battery applications. *Electrochem. commun.* **2015,** *60*, 121-125.
21. Khamsanga, S.; Pornprasertsuk, R.; Yonezawa, T.; Mohamad, A. A.; Kheawhom, S., δ-MnO2 nanoflower/graphite cathode for rechargeable aqueous zinc ion batteries. *Sci. Rep.* **2019,** *9* (1), 8441.